Primljen / Received: 29.12.2025.
Ispravljen / Corrected: 28.4.2026.
Prihvaćen / Accepted: 12.5.2026.
Dostupno online / Available online: 10.5.2026.

# Numerical investigation of barge collision with a bridge column

Authors:

Prof. **Hrvoje Draganić**, PhD. CE
Josip Juraj Strossmayer University of Osijek
Faculty of Civil Engineering and Architecture Osijek
draganic@gfos.hr
**Corresponding author**

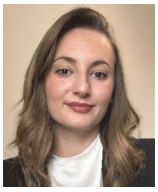

**Etna Marković**, MCE
RC Consulting d.o.o., Croatia
markovicetna@gmail.com

Assist.Prof. **Mario Jeleč**, PhD. CE
Josip Juraj Strossmayer University of Osijek
Faculty of Civil Engineering and Architecture Osijek
mjelec@gfos.hr

**Research Paper**

Hrvoje Draganić, Etna Marković, Mario Jeleč

## Numerical investigation of barge collision with a bridge column

A vessel-bridge collision can result in severe loss of life and substantial damage. This study presents a numerical analysis of the vessel impact on a column of the Ilok-Bačka Palanka bridge in Croatia. Using finite element modelling, different barge–column interactions under multiple loading conditions were simulated. The numerical model includes realistic vessel and bridge-pier geometry, as well as material behaviour. The numerical simulation results were compared with the damage caused to the column after the impact. The column damage was evaluated using a concrete degradation modelled via an erosion-based algorithm driven by instantaneous geometric strain. The calibrated numerical model was also used in a parametric analysis to determine the influence of the impact direction and speed on the observed bridge pier.

**Key words:**
**vessel collision, case study, bridge column, numerical analysis, concrete degradation**

**Prethodno priopćenje**

Hrvoje Draganić, Etna Marković, Mario Jeleč

## Numeričko istraživanje udara plovila u stup mosta

Udar plovila u most može rezultirati teškim gubitkom života i znatnom štetom. Rad predstavlja numeričku analizu studije stvarnog slučaja udara plovila u stup mosta Ilok – Bačka Palanka 2024. godine u Hrvatskoj. Primjenom metode konačnih elemenata simulirane su različite interakcije između plovila i stupa pod variranim uvjetima opterećenja. Numerički model uključuje realističnu geometriju plovila i stupa mosta kao i ponašanje materijala. Rezultati numeričke simulacije uspoređeni su s oštećenjima prouzročenim na stupu nakon udara. Oštećenje stupa procijenjeno je oštećenjem betona kroz modeliranje efekta erozije koji definira trenutna geometrijska deformacija. Kalibrirani numerički model dodatno je korišten u parametarskoj analizi u svrhu utvrđivanja utjecaja smjera i brzine udara u promatrani stup mosta.

**Ključne riječi:**
**udar plovila, studija slučaja, stup mosta, numerička analiza, degradacija betona**

## 1. Introduction

A vessel colliding with a bridge column can cause severe human casualties and material damage. Bridges are critical links in modern transportation, and their ability to withstand impact loads is crucial to maintaining safe, uninterrupted traffic flow. As river and sea traffic increases, so does the risk of collisions, raising concerns about the stability and resilience of bridge structures. Each impact poses an immediate threat and adds cumulative stress, potentially compromising safety and longevity. Vessel-bridge collision accidents have caused numerous bridge failures [1], with 35 cases worldwide recorded from 1960 to 2015, resulting in hundreds of fatalities [2]. Analysis shows that bridges with a main span shorter than two to three vessel lengths or two channel widths are particularly vulnerable [3]. Vessels in ballast are highly affected by wind and currents, and barges, especially near bends or in strong currents, are challenging to manoeuvre, often sliding in the opposite direction of a turn. Bridges near channel bends or on high-speed waterways face a higher risk of frequent barge impacts.

Design standards, such as Eurocode [4] and those issued by the American Association of State Highway and Transportation Officials [5] provide guidelines for bridge design to mitigate the risk of vessel collisions. These standards often use empirical formulas to calculate equivalent static forces during collisions. However, vessel-pier collisions are inherently dynamic events characterised by intense energy exchanges between the vessel and the bridge structure over a short duration. Static analysis procedures overlook critical dynamic amplification effects, such as superstructure inertial responses, potentially underestimating collision loads and structural demands [3, 6].

Simulating vessel-bridge collisions typically requires complex nonlinear dynamic analyses. These collisions, occurring within seconds, generate significant lateral forces that propagate from the impact area to other bridge components, including piles and superstructures. Numerous studies have explored the nonlinear dynamic behaviour of bridges under vessel impact through analytical, numerical, and experimental approaches. A few experimental tests on vessel-bridge collisions have been conducted (e.g. [7, 8]), but they face notable challenges. Full-scale tests are often prohibitively expensive, time-consuming, and impractical, while reduced-scale model tests in laboratories are limited by scaling effects in structural geometry [9, 10]. Contact-based finite element (FE) methods offer a viable and practical alternative to address these limitations. However, developing a finite element analysis (FEA) model of a colliding vessel can be time-intensive, requiring significant computational and modelling effort.

In recent years, several studies have extensively explored various influences of vessel-bridge collisions, with particular emphasis on critical aspects such as impact forces [10-12] or the progressive collapse mechanisms of bridges [13]. These investigations have contributed to crucial factors, including the mass and velocity of vessels, the structural stiffness of bridges, the presence of superstructures, and the dynamic interactions between the colliding vessel and the impacted structure [11]. One noteworthy study by Sha and Hao [10] investigated the critical role of column geometry, demonstrating its significant impact on the magnitude and distribution of collision forces. Their research highlights how the design of column shapes can influence structural resilience during impacts. Experimental research by Kantrales et al. [14] further supports these findings, showing that barge impact forces are significantly reduced when targeting rounded bridge elements rather than flat-faced ones with equivalent geometric dimensions. Several other studies [15, 16] have investigated the influence of soil-structure interaction (SSI) on vessel-bridge collisions, showing that changes in soil conditions can significantly affect the bridge response to collisions.

Many researchers have studied the nonlinear dynamic behaviour of the vessel-bridge system during collision events by performing high-resolution FE simulations [17-19]. Other methods, such as the response spectrum method [20, 21], have also been used to estimate the collision-induced bridge response. Recent studies have focused on developing anti-collision protective measures, such as applying protective bonded steel plates [22] and foam-filled lattice composite bumper systems [23]. The works mentioned above have contributed to a better understanding of the nonlinear dynamic vessel-bridge interaction during a collision event. However, high-resolution FE simulations are usually computationally demanding. To reduce computational costs, several researchers have proposed simplified methods for vessel-bridge collision analyses [24-26]. However, as mentioned earlier, a simplified approach must be carefully applied, as vessel-pier collisions are inherently dynamic and involve several influencing parameters that should be considered in the simplification.

The paper presents a case study of a 2024 vessel collision with the Ilok-Bačka Palanka bridge column to perform a detailed numerical FE analysis of the accident. The paper focuses on developing a numerical model of the column-and-barge vessel, as described in the bridge's existing project documentation and AASHTO standards. The simulations were conducted using Ansys 2024 R2 [27], enabling a detailed assessment of the structural response to dynamic loading. Different vessel-bridge interactions under various impact scenarios were simulated to assess damage caused by barge bow impact. The analysed event is treated as a case-based numerical reconstruction of a real collision for which only limited post-event information was available. Therefore, the objective of the study is not a full forensic identification of all collision parameters, but rather an assessment of whether a physically reasonable finite element model can reproduce the observed local damage pattern of the impacted bridge column and provide a basis for comparative investigation of several representative impact scenarios. The presented results should therefore be interpreted within the framework of the adopted assumptions regarding geometry, material properties, contact formulation, and available field observations.

## 2. Case study

### 2.1. Bridge geometry

The Ilok–Bačka Palanka bridge, extending 725 meters, was constructed in 1974 to provide a direct connection between the right and left banks of the Danube River near Bačka Palanka (Figure 1). This bridge was designed to facilitate both vehicular and pedestrian traffic, supporting regional connectivity and economic activities. The bridge geometry was taken from the main project in the State Archives in Zagreb [28]. The cross-sectional width of the bridge structure is 10.9 meters, comprising a 7.5-meter-wide vehicular traffic lane and two-way pedestrian pathways 1.5 meters wide on each side, allowing pedestrians to pass safely (Figure 2).

The bridge features a central opening designed explicitly for river navigation. This navigational channel spans 150 meters in width and provides a vertical clearance of 9.5 meters above the maximum navigable water level, which is positioned at an elevation of 80.11 meters. This clearance is essential for the safe passage of ships and barges along the Danube. The superstructure of the bridge consists of two units: an inundation composite system of simple beams with spans of 6 × 60 m, and the main steel structure in the form of a continuous beam with spans of 100.0 + 160.0 + 100.0 m.

**Figure 1. Ilok - Bačka Palanka bridge**

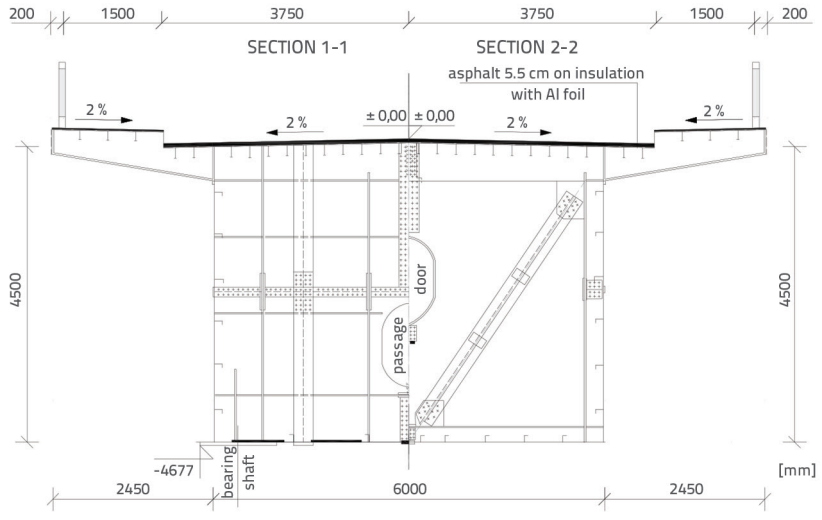


**Figure 2. Cross sections of the bridge superstructure [28]**

The inundation composite girders are box-sectioned and covered with prefabricated reinforced concrete (RC) slabs. The steel box structure has a constant height along its entire length, measuring 2700 × 5490 mm. The sheets of ribs and bottom steel plates are 12 mm and 16 mm thick, respectively. The RC slab is made of concrete grade MB400, as per the former regulations for composite structures.

The main steel structure features a box-shaped rectangular section with an orthotropic plate on top, as shown in Figure 2. The box and plate widths are 5.94 m and 10.9 m, respectively. The vertical sheet height in the middle opening is 4.5 m, while in the end openings it varies linearly from 3.0 m to 4.5 m at the middle supports. The main girder is constructed in a vertical curve with a radius of 10,000 meters and a longitudinal slope of 0.8 %. In the transverse direction, the traffic surface is constructed with a 2 % slope on both sides towards the structure's edges. The plate on the traffic surface is made of 12 mm sheet metal, while on the pedestrian paths, metal sheets 10 mm and 16 mm thick are used, respectively. The vertical walls of the box are made of 12 mm and 14 mm thick steel sheets, and near the supports, they are 25 mm thick. Steel fences are 1.0 m high. Steel grade St37 was mainly used for the superstructure, while St52 was used only for the longitudinal elements supporting the main and cross girders above the columns. Dimensioning of the steel structure was carried out in accordance with DIN 1073 and DIN 4114, as well as the former regulations for composite structures.

The bridge's substructure consists of 10 columns, of which columns 1 to 7 are located under the inundation part and columns 8 - 10 under the main structure, as shown in Figure 3. The column affected by the impact is number 8. Four tall columns support the main structure, and only one, column 8, has a fixed bearing. All columns are made of solid reinforced concrete sections, MB300. In the central opening and the fairway, two columns (8 and 9) are built on concrete caissons and are approximately the same size and shape, as shown in Figure 4. Bridge columns consist of two different cross-sections positioned with respect to the water level. The column body's lower part, which is submerged at normal and high-water levels, is shaped as a diamond to provide minimal resistance to water flow, thereby reducing erosion of both the column material and the foundation soil. The upper part of the column body is rectangular because a very high-water level is assumed to be infrequent. Its occurrence would not severely damage columns positioned in the riverbed.

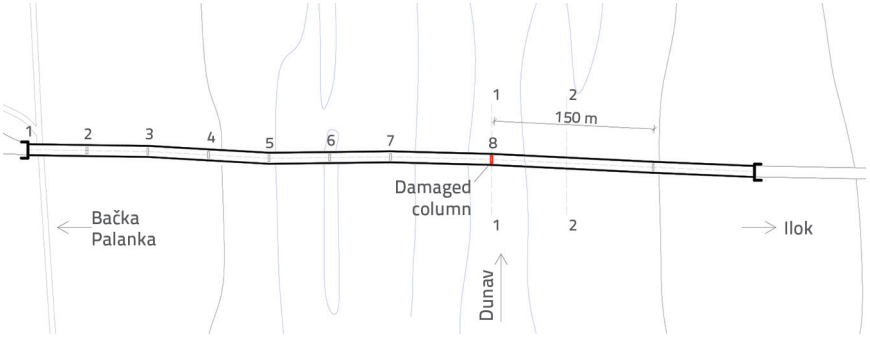


**Figure 3. The longitudinal column disposition of the bridge [28]**

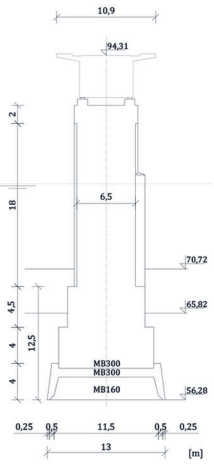


**Figure 4. Geometry of the considered column [28]**

The geometry presented in this study was derived from the available original technical documentation and subsequently compared with photographs from the inspection performed after the collision. It was observed that the constructed lower part of the column differs from the original drawings due to a locally thickened outer concrete zone. Since no complete as-built documentation of this modification was available, the numerical model was developed using the documented original geometry. At the same time, the observed discrepancy was explicitly considered when discussing the agreement between the numerical results and the recorded field damage.

The dimensions of the column's cross-section are 2 × 6.5 m. On the upstream side, there are also concrete ice breaks up to 1 m above the maximum navigable water level (81.11 m), 1 m thick, reinforced at the top with steel angles. Above the ice break on the upstream and downstream sides, the columns are bevelled by 25 cm. The 13 x 7.5 m caissons are lowered into artificial gravel embankments. The height of the artificial embankments is 76.85 m, that is, 1 m above the mean water level.

## 2.2. Load case scenario

The most common vessels on the Danube waterway are cruisers, self-propelled cargo ships, and pushers and thrusters. Due to the advantages of propulsion, towing is almost entirely omitted on inland waterways. The pressurised composition consists of pushers and thrusters (barges) that can be arranged in one or more rows. The thrusters are 60 to 110 m long and have a load capacity of 1700 tons. The maximum width of the vessel is 11.4 m due to the existence of locks on waterways, which, due to their shape, do not allow greater widths. The average speed of vessels downstream of the Danube ranges from 15 to 20 km/h, and upstream from 7 to 10 km/h, with no specific rules prescribing maximum navigation speeds [29].

In the considered load case scenario, barge *Antonia*, transporting two fully loaded barges, navigated the Danube River from Linz to Smederevo when it unexpectedly deviated from the designated waterway. As shown in Figure 5, the vessel, with an approximate speed of 15 km/h, collided with a column of the Ilok–Bačka Palanka road bridge at an angle of 20° measured perpendicular to the bridge axis [29]. This impact caused a significant breach in the ship's hull, resulting in the sinking of one barge loaded with approximately 1,000 tons of artificial fertiliser. Due to the cargo's nature and the waterway's environmental sensitivity, immediate protective measures were required to mitigate potential ecological harm from the submerged fertiliser. Additionally, vehicular traffic on the bridge was halted due to the risk posed by the impact damage. Upon thorough inspection, authorities implemented strict traffic restrictions on the bridge. These included a maximum permissible vehicle weight of 24 tons, a speed limit of 30 km/h, and a prohibition on stopping on the bridge to minimise stress on the compromised structure. Observed damage is depicted in Figure 5, showing the condition of the impacted column. Later, a detailed inspection indicated no damage to the span assembly or the column foundation. As shown in Figure 5, the collision occurred in the lower part of the column body. Based on visual observation, the damage to the column was classified as superficial, as the erosion of the concrete protection layer exposed the reinforcement bars to environmental influences, but did not endanger the overall bridge stability. Relatively small, superficial damage of the column and no damage to the superstructure indicate a low-energy collision.

Overall, as described in this section, the available data for the described collision were limited to the identified vessel type, the traffic and inspection reports, the estimated vessel speed provided by the competent authority, and photographic records of the damaged column. Detailed measurements of the vessel bow after impact, direct records of impact force, structural accelerations, displacements, or time-history response of the bridge were not available. For this reason, the real event was used primarily as a reference case for comparing the location and extent of visible local damage rather than for a strict quantitative validation based on measured response histories.

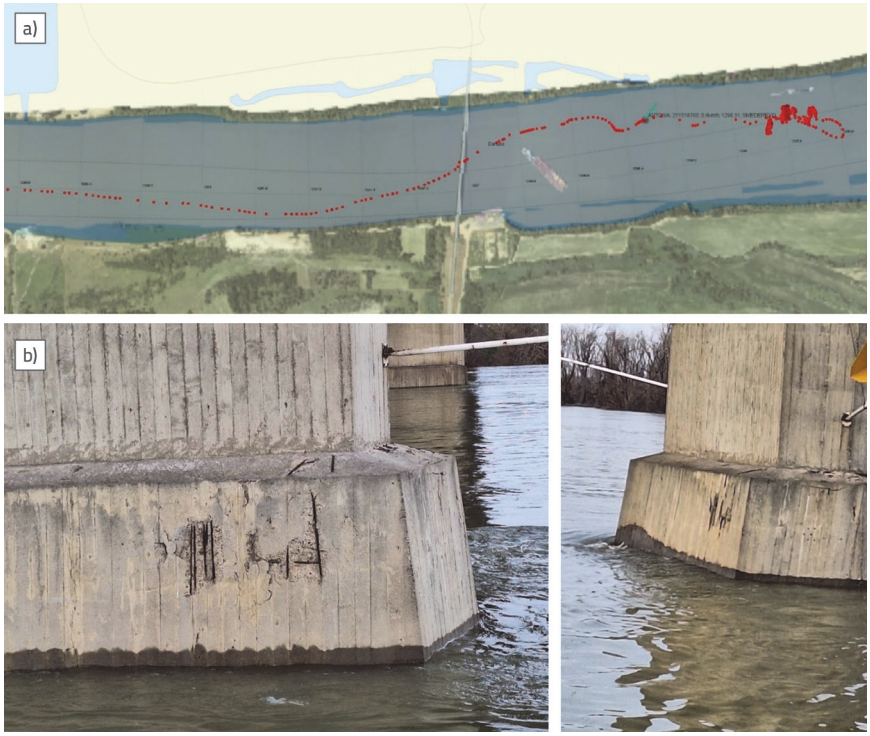


**Figure 5. a) Vessel trajectory ; b) damaged bridge column [29]**

## 3. Numerical modelling

The primary focus of the numerical model is to simulate a vessel-bridge collision using data from an actual collision recorded on the subject bridge.

### 3.1. Model geometry

The model geometry of the impacted column was created based on the geometry provided in the technical drawings. However, a slight deviation in geometry can be observed between the in-situ column (Figure 4) and those depicted in the technical drawings (Figure 6).

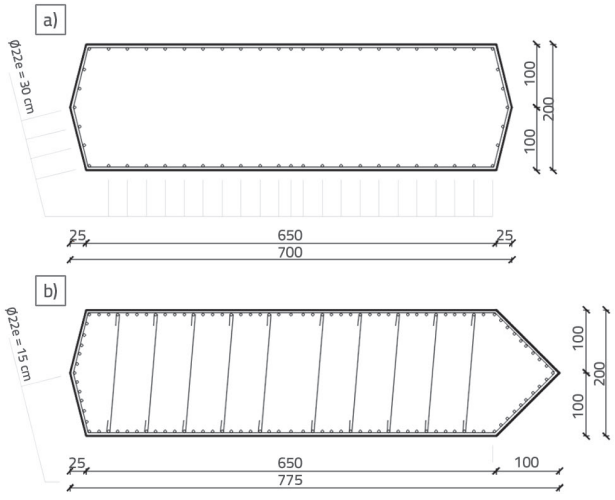


**Figure 6. Column cross-sections: a) upper part of the column; b) lower part of the column**

Since the exact geometry of the site column was unknown, the technical drawings served as the basis for the model geometry, as mentioned already in the previous section. Based on the geometry provided in the technical drawings, the impacted column was modelled using beam and solid elements. Solid elements were used to model the concrete part of the column, while beam elements were used to model reinforcement bars. The column's shape was carefully modelled to reflect its actual shape. Initially, the whole height of the column was modelled (Figure 7.a); however, to simplify the model and taking into account no observed damage in the span assembly or at the column foundation, it was decided to reduce the column model size by removing the column foundation and the massive concrete part extending from the foundation that transforms into a column cross-section as described in the previous section (Figure 7.b).

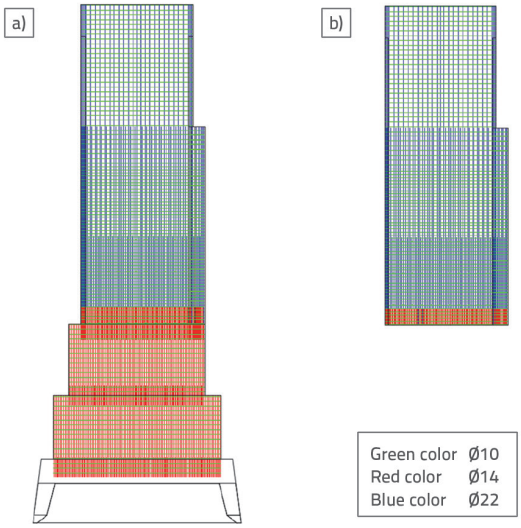


**Figure 7. Numerical model of a column: a) entire model; b) reduced model**

The adopted column model was intentionally focused on the region relevant for local impact response. The retained geometry includes the impact zone, the transition of the column cross-section, and the base widening, which governs local force transfer in the analysed model. The lower part of the pier and the foundation system were not explicitly modelled because the study's objective was to investigate local damage development in the impact region rather than the global soil–foundation response. This idealisation is therefore a modelling assumption and should be interpreted as one of the study's main limitations.

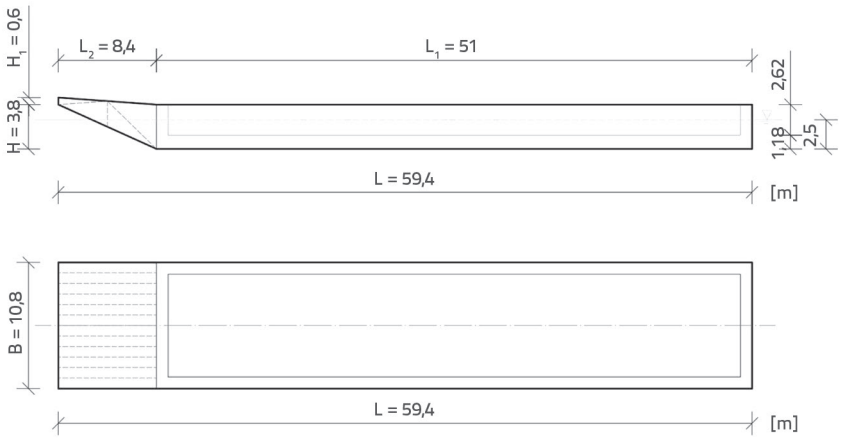


**Figure 8. Barge geometry**

Regarding the vessel's geometry, as mentioned in Section 2, in the considered case, the pusher assembly consists of pushers and barges that can be stacked in one or more rows, with lengths varying from 60 to 110 m and a maximum width of 11.4 m. Due to the predominance of thrust compositions on the Danube, a vessel with a load capacity of 1700 tons was used in this paper for impact simulation. The dimensions are based on the AASHTO standards [5] for standard bulk thrusters, as shown in Figure 8 and Table 1.

**Table 1. Adopted dimensions of the standard bulk barge with a load capacity of 1700 tons**

| | **AASHTO** [ft] | **Adopted dimensions** [m] |
|---|---|---|
| Width | 35 | 10.8 |
| Length | 195 | 59.4 |
| Depth | 12 | 3.8 |
| Height of storage space | 8.7 | 2.62 |

The isometric spatial representation of the barge bow is shown in Figure 9. A 30 mm thick steel sheet is used for the barge body. Accordingly, the barge body has a volume of approximately 52.37 m$^3$.

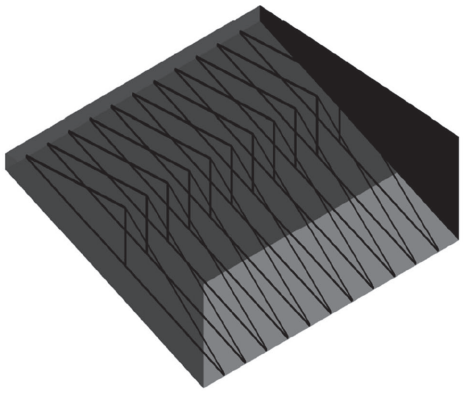

**Figure 9. Isometric spatial representation of the barge bow**

Since the density of steel is 7830 kg/m$^3$, the mass of the barge body is 410 tonnes. Since detailed construction drawings of the barge bow were not available, the internal stiffening of the bow structure was represented in an idealised manner consistent with the typical arrangement of this vessel type. The additional steel mass was therefore introduced as a modelling assumption to account for the presence of internal stiffeners, resulting in a total barge mass of 535 tonnes. To reduce model complexity, this mass was converted into a solid element representing the barge body. Considering the short duration of the analysed impact event, no substantial redistribution of stresses outside the immediate bow impact region was assumed in the simplified barge model. The total weight of the thruster, including the body and bow, is approximately 600 tonnes. For ease of calculation, the internal complex structure of the bow is simplified by placing 11 lattice systems at a distance of 90 cm from each other, as shown in Figure 9. The adopted thickness of the lattice elements and the bow plate is 30 mm, while the height of the lattice elements is 100 mm.

## 3.2. Mesh size, contact elements and boundary conditions

Numerical results are sensitive to the size of the finite element mesh. Since it is a complex model, a minor division of finite elements would cause the computer program to crash due to limitations in processing capacity and working memory. In a preliminary parameter study, the mesh size was varied from 75 to 200 mm. To maintain numerical stability and optimise computational time, a mesh size of 125 mm was chosen for the surfaces in direct contact. A mesh size of 250 mm is adopted for the rest of the model.

The concrete material part of the column was modelled as a solid element, while the reinforcement bars were modelled as beam elements. Solid elements are of finite element type Hex8 (SOLID65), i.e., linear eight-node hexahedron elements shaped as an eight-node brick (eight integration nodes on each corner of a finite element). Beam formulations were selected for steel reinforcement to model bending behaviour during interaction with the RC column during lateral vessel collision. The contact algorithm converts beam elements into reinforcement bars (LINK8) and enables ideal coupling, ensuring an ideal bond between the concrete and reinforcement bars. In the algorithm, reinforcement bars are used to maintain beam characteristics during analysis. The steel material part of the vessel was modelled as a shell element (SHELL163 and SHELL209). Additionally, the bow shell elements in the lattice system and the bow with the thruster body are connected using a rigid (bonded) contact algorithm.

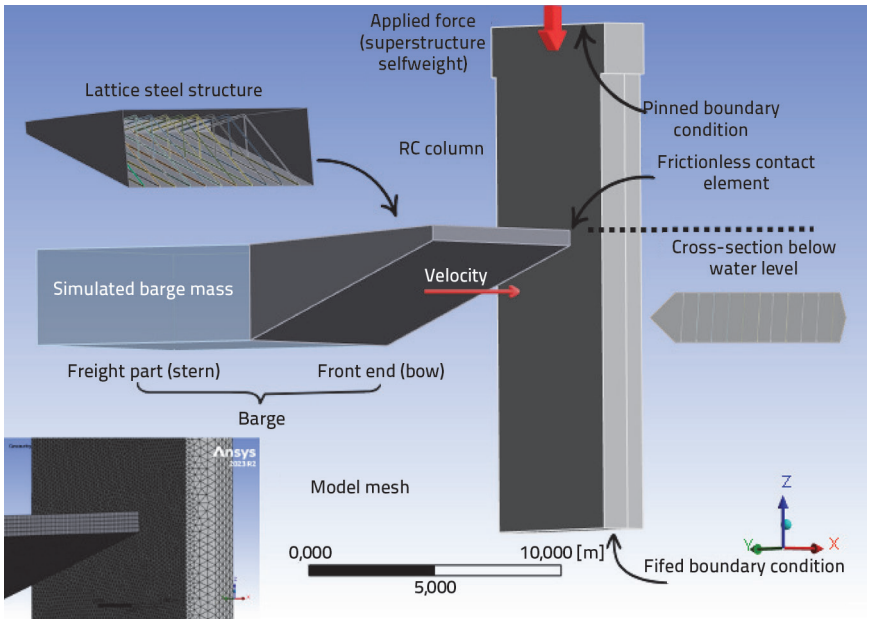


**Figure 10. Numerical model of vessel-column collision**

Several contact algorithms are introduced in the model. In the real load scenario, the vessel's bow and the column are joined through two variations of contact elements, i.e., frictional or frictionless. In both contact formulations, the bow's side and bottom shell elements act as the contact surfaces, and the column's impact surface is defined as the target, depending on the case. In a preliminary study, the friction coefficient was varied from 0.30 to 0.60, and 0.45 was selected for the frictional contact elements between steel and concrete, in accordance with the literature [30–33].

Two contact idealisations were examined in the reference collision case to evaluate their influence on the predicted damage pattern. The frictional model is physically more representative of steel–concrete interaction during sliding contact; however, in the present simulations, it led to premature termination of the analysis due to numerical instability after the bow was embedded locally into the concrete surface. The frictionless contact formulation is therefore not introduced as a physically superior representation of the real event, but as a numerically robust approximation that enables complete simulation time and consistent comparison between the analysed impact scenarios. The results obtained with this formulation should be interpreted accordingly.

In the numerical model, two principal simplifications were adopted concerning the boundary conditions and the representation of the superstructure. Since the available field observations indicated localised surface damage concentrated at the impact zone, the model was formulated to capture the local collision response of the pier rather than the full dynamic behaviour of the bridge–foundation system. Accordingly, the pier base was idealised as fully fixed, while the top of the model was constrained in a simplified manner to represent the restraint provided by the superstructure. The superstructure was represented by its equivalent resultant vertical load, calculated from the documented cross-section dimensions and material characteristics, which amounted to 5670 kN. This simplification does not reproduce the full bearing-level load transfer mechanism or the superstructure's inertia, but it enables a numerically stable representation of the axial compression acting on the column during the collision analysis. The influence of these assumptions should be taken into account when interpreting the results.

The vessel's speed of 15 km/h was adopted following the Port Authority's assessment. A summary of the numerical model of vessel-column collision, with the most critical parameters, is shown in Figure 10.

### 3.3. Material parameters

Concrete behaviour was modelled using the RHT [34] (Riedel-Hiermaier-Thoma) material model, which includes the necessary features to describe concrete's dynamic strength at impact-relevant velocities accurately. The RHT concrete model is an advanced plasticity model used for simulating the dynamic loading of concrete, especially for brittle materials. This model combines plasticity and shear damage to limit the material's deviatoric stress via a generalised failure surface. It is designed to be modular, allowing for specific aspects of material behaviour to be activated or deactivated, making it highly practical for various applications. Ansys 2024 R2 [27] contains predefined parameters for the RHT concrete model with a compressive strength of 35 MPa. Table 2 presents the corrected parameters for the concrete class C25/30, as implemented in the concrete material model for column 8. The advantage of the RHT concrete model is its adaptability to different material strengths, as strength changes are reflected in recalculated values based on the defined material parameters. The concrete grade was obtained from the original technical specification, MB300, corresponding to compressive strength class C25/30, as specified in EN 206-1:2026 [35]. Concrete degradation was modelled through an erosion-based element deletion algorithm governed by instantaneous geometric strain. In a preliminary parameter study, the erosion factor was varied within 0.3 to 0.7. However, the observed damage in the numerical model was influenced not only by the erosion factor but also by the mesh size. Therefore, a pair of values was analysed. In that sense, elements were removed from the mesh when their strain exceeded the chosen threshold of 0.5 to ensure numerical stability and reflect material failure. The selected erosion parameter is chosen within the limits given in the literature [36, 37]. Since the adopted concrete class was based on the available original project documentation, no destructive or non-destructive in-situ testing data were available for the present study, and therefore, the material model could not be calibrated

**Table 2. RHT concrete material model used in the simulations [27]**

| Parameter | Description | C25/30 |
|---|---|---|
| $G_{el}$ | Elastic shear modulus | 16.7 GPa |
| $f_c$ | Static compressive strength of concrete | 25.0 MPa |
| $f_t/f_c$ | The ratio of static tensile and compressive strength of concrete | 0.104 |
| $f_s/f_c$ | The ratio of shear and static compressive strength of concrete | 0.18 |
| $A_{fail}$ | Pressure-independent parameter for the failure surface | 0.00 |
| $B_{fail}$ | Linear parameter for the failure surface | 1.60 |
| $N_{fail}$ | Failure surface exponent | 0.61 |
| $Q_{2.0}$ | The ratio of tensile and compressive meridians. reference value | 0.6805 |
| $B_Q$ | Parameter of transition from brittle to ductile behaviour | 0.0105 |
| $G_{el}/(G_{el}-G_{pl})$ | The ratio of the elastic shear modulus and the difference between the elastic and plastic shear modulus | 2.0 |
| $f_{t,el}/f_t$ | The ratio of elastic and static tensile strength of concrete | 0.7 |
| $f_{c,el}/f_c$ | Ratio of elastic and static compressive strength of concrete | 0.53 |
| Cap option | Peak value option | Active |
| $B_{frac}$ | Linear parameter for the residual strength surface | 1.60 |
| $N_{frac}$ | Exponent of the residual strength surface | 0.61 |
| A | Compressive strength increase exponent | 0.032 |
| **Δ** | Tensile strength increase exponent | 0.036 |
| $D_{RHT1}$ | $D_1$ material damage parameter | 0.04 |
| $D_{RHT2}$ | $D_2$ material damage parameter | 1.00 |

**Table 3. Steel parameters according to the Johnson and Cook mode [27]**

| Parameter | Description | STEEL 4340 |
|---|---|---|
| $G$ | Shear modulus | 81800 MPa |
| $f_y$ | Yield strength | 240 MPa |
| $B$ | Hardening modulus | 500 MPa |
| $n$ | Work-hardening exponent | 0.26 |
| $C$ | The strain rate hardening | 0.014 |
| $m$ | Thermal softening coefficient | 1.03 |
| $T_{melt}$ | Temperature of melting | 1519.9 °C |

against measured concrete properties from the existing structure. For the same reason, possible long-term changes in material properties due to ageing, environmental exposure, or local deterioration were not introduced explicitly into the numerical model. The adopted material parameters should thus be understood as representative design-based values suitable for a comparative numerical study, rather than as directly measured in situ properties of the bridge column at the time of collision. During the available post-event visual inspection, no indications were reported of extensive concrete deterioration, reinforcement exposure outside the impact zone, or damage to the foundation and superstructure that would suggest severe pre-existing structural degradation. Nevertheless, because no dedicated durability assessment, corrosion survey, or materials testing campaign was available, the possible influence of such effects cannot be quantified within the present study and remains outside its scope.

For the steel model, STEEL 4340 was selected, with its parameters defined in Ansys 2024 R2 [27]. The Johnson-Cook model [38] is used for calculations requiring high steel strength, such as impact resistance, plastic flow, thermal softening, and deformation rate; see the steel model parameters in Table 3. The values shown in Table 3 have been corrected for reinforcing steel GA 240/360. This steel model has also been adopted for the thruster material.

Johnson and Cook proposed an empirical model to describe the plastic deformation and damage of steel at various speeds and temperatures. The model uses an equation to describe the stress-strain relationship:

$$\sigma = [A + B_{\varepsilon}^{n}][1 + C\ln\dot{\varepsilon}^{*}][1 - (T^{*})^{m}] \quad (1)$$

where $A$, $B$, $n$, $C$ and $m$ are the material parameters, $\varepsilon$ plastic deformation, $\dot{\varepsilon}^{*}$ normalised deformation rate, and $T^{*}$ is the normalised temperature.

## 4. Results and discussion

### 4.1. Real load scenario

Results of the real load scenario of the vessel–column impact are discussed in this section. Model validation was performed by comparing the simulated damage pattern with the observed field damage from the real incident. No quantitative field records, such as impact force, displacement, acceleration, or strain histories, were available since no measuring devices were installed on the bridge at the time of the event. Therefore, validation is limited to comparing the location, shape, and extent of the visibly damaged zone recorded during the post-event inspection. Figure 11 and Figure 12 show the resulting damage to the column for two cases of vessel–column contact, i.e. frictional and frictionless, respectively. In the real load scenario, the barge impacted the column at approximately 20°, resulting in an edge impact on the strengthened column section. The numerical simulation attempted to reproduce this event using the available geometric, material, and operational information. As noted previously, the model was based on the original technical

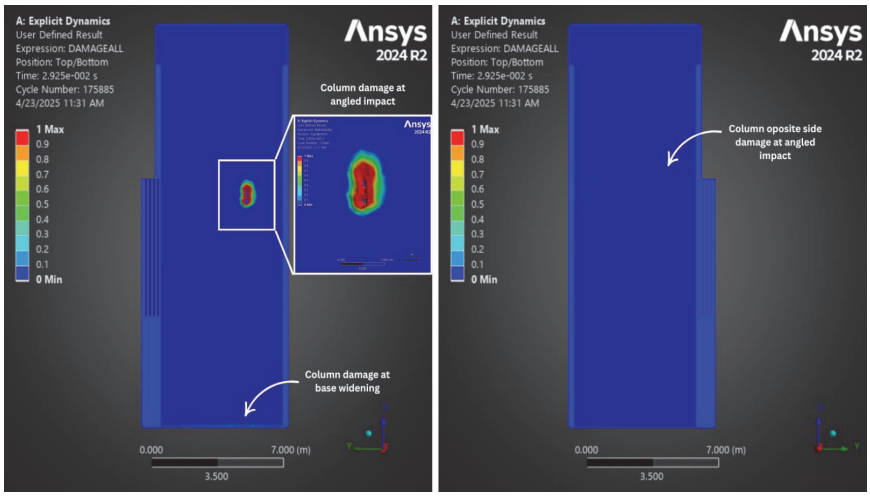


**Figure 11. Simulated column damage - frictional model**

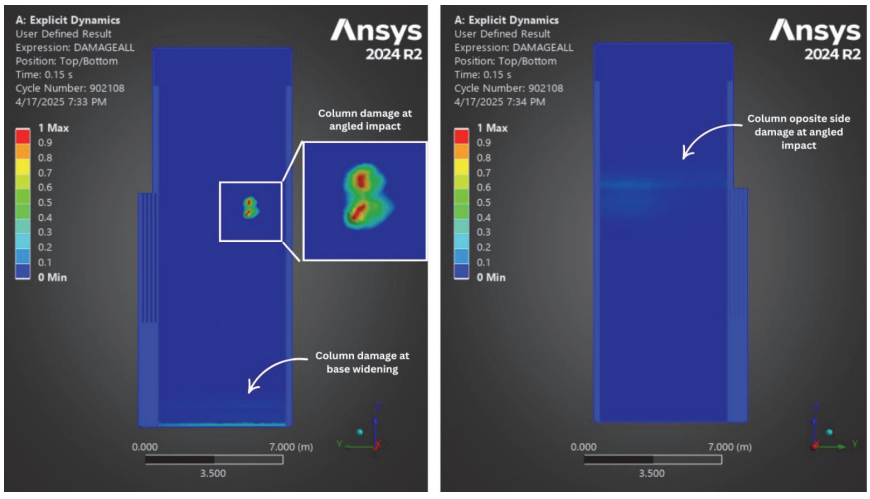


**Figure 12. Simulated column damage - frictionless model**

documentation; however, subsequent inspection indicated that the lower part of the constructed column differs from the original geometry due to local strengthening. Therefore, numerical results provide an additional safety margin. This discrepancy is also one of the reasons why the comparison with the observed damage should be interpreted qualitatively rather than as a strict quantitative validation.

Both frictional and frictionless models indicate localised damage at the impact point, but their physical interpretation differs. In the frictional model, sliding occurs with tangential resistance, leading to local embedding of the bow into the column and the removal of the concrete cover, with partial exposure of reinforcement bars, as shown in Figure 11. In terms of visible damage pattern, this response is closer to the field observations. However, due to the pronounced local nonlinearity that develops after contact, the frictional simulation became numerically unstable and terminated after approximately 30 ms. In contrast, the frictionless model permits sliding and separation without tangential resistance and therefore remains numerically stable during the full 150 ms simulation time. This model predicts some aspects of the response less realistically, particularly the rebound tendency after impact, but it provides a stable basis for comparative assessment of the additional impact scenarios presented in the following section. For this reason, the frictionless formulation was retained for the parametric comparison, while the frictional model was used primarily as a qualitative indicator of the likely local damage mechanism in the real collision.

Further comparisons for the two considered cases of vessel-column contact are presented in Figure 13 based on the reaction forces at the column base widening. The frictional model stops at 30 ms due to numerical instability, at which point the bow edge embeds into a concrete column. The frictionless model rebounds, reducing potential numerical instability, and consequently, the model finishes calculation within 150 ms. The maximal force reaction at base widening was 42 MN for the frictionless model, whereas it was 21 MN for the frictional model. Even if the frictional model did not reach its designated calculation time, the reaction force value aligns well with the frictionless model, as shown in Figure 13. Since the frictional model allows more energy dissipation through sliding and embedding, a lower reaction force value would be expected for a designated 150 ms.

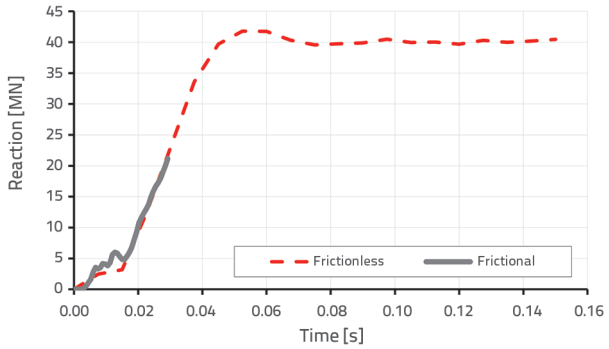


**Figure 13. Reaction forces at the column base widening for the considered cases**

Figure 14 and Figure 15 show the resulting normal stress on the vessel's bow at impact for two cases of vessel-column contact, i.e. frictional and frictionless. Both models indicate very similar damage and stress distribution. As expected, the bow impact edge has the most significant stresses, with indentation of the bow edge at impact. The bending of steel

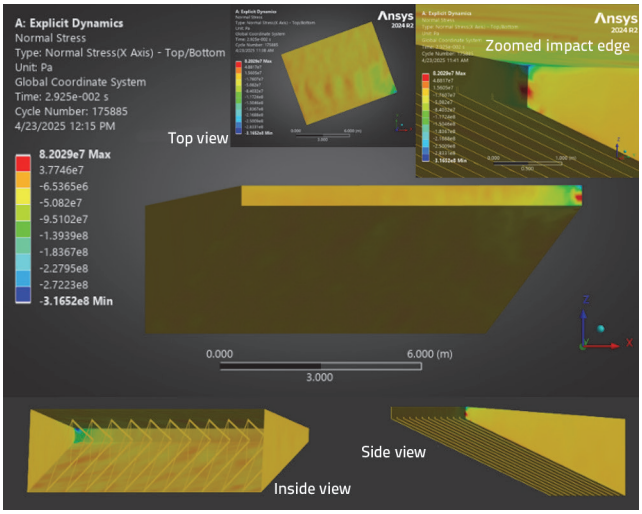


**Figure 14. Bow normal stresses at impact – frictional model**

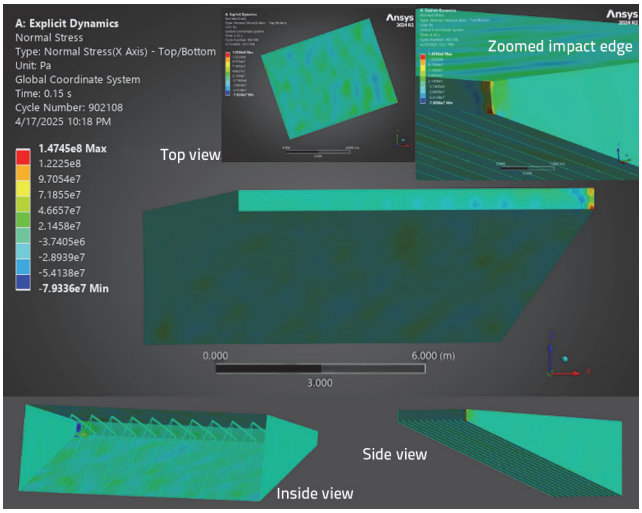


**Figure 15. Bow normal stresses at impact – frictionless model**

lattice elements supporting bow steel plates is pronounced on the impact side.

## 4.2. Load case scenarios

To investigate other possible load case scenarios, three barge position cases with varying navigation direction and impact angle are examined. Case A represents a head-on impact of the barge downstream of the Danube. In the case of B, a frontal impact is also observed, but in the upstream direction of navigation of the barge. Case C represents an angled impact perpendicular to the column's bevelled reinforcement surface in the navigation's downstream direction.

**Table 4. Observed impact cases**

| Case | Thruster position | Impact characteristics | |
|---|---|---|---|
| A | 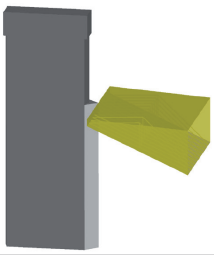 | Maximum point of impact | 81.12 m |
| | | Water level | 79.22 m |
| | | Type of impact | front |
| | | Direction of navigation | downstream |
| | | Navigation speed | 4.2 m/s |
| B | 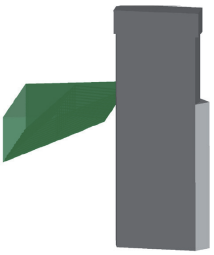 | Maximum point of impact | 81.12 m |
| | | Water level | 79.22 m |
| | | Type of impact | front |
| | | Direction of navigation | upstream |
| | | Navigation speed | 2.0 m/s |
| C | 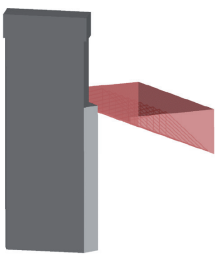 | Maximum point of impact | 81.12 m |
| | | Water level | 79.22 m |
| | | Type of impact | angled |
| | | Direction of navigation | downstream |
| | | Navigation speed | 4.2 m/s |

The described cases are shown in Table 4. For the downstream navigation direction, a speed of 15 km/h was adopted, corresponding to approximately 4.2 m/s, the same as in the real load scenario, while for the upstream direction, a speed of 7 km/h, or 2 m/s, was adopted, all following the regulations [29]. Because the frictional contact formulation in the reference real-load simulation led to premature numerical instability, all three additional load case scenarios (A, B and C) were analysed using the frictionless contact formulation to ensure complete, mutually comparable simulations. Even if rebounds occurred in a real load scenario, they would not happen in the considered load case scenarios due to a much higher hitting angle between

**Table 5. The course of damage to the column for the considered cases**

| **Time** [s] | **Case A** | **Case B** | **Case C** |
|---|---|---|---|
| | 1 0,5 0 Max Min | | |
| 0.05 | 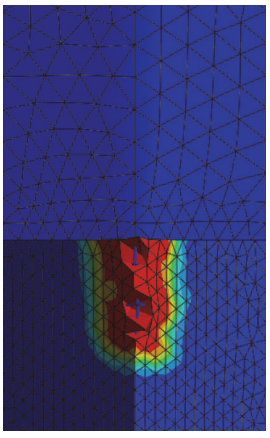 | 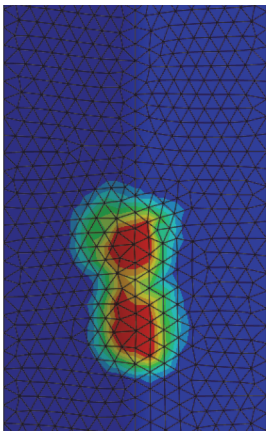 | 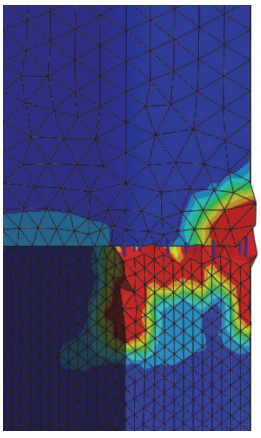 |
| 0.10 | 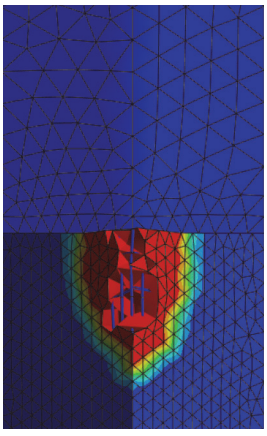 | 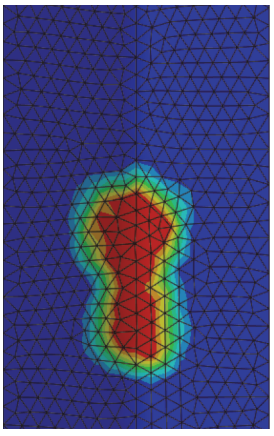 | 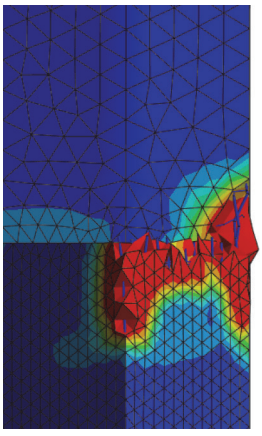 |
| 0.15 | 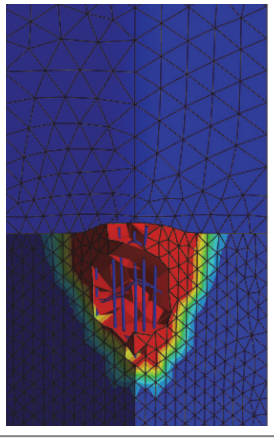 | 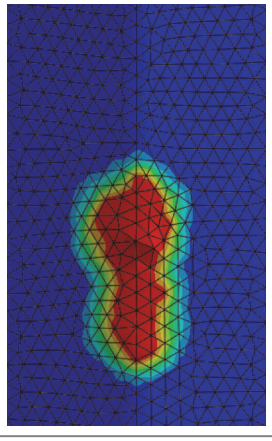 | 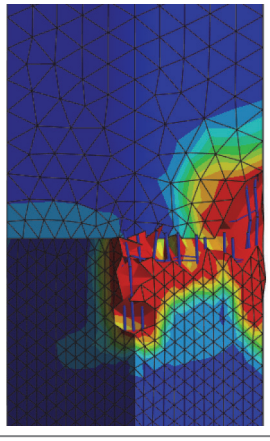 |

**Table 6. Reinforcement yielding for the considered cases**

| | *Case A* | *Case B* | *Case C* |
|---|---|---|---|
| Time [s] | 0.15 | - | 0.08 |
| Reinforcement type | transverse | - | transverse, longitudinal |
| Place of yielding | 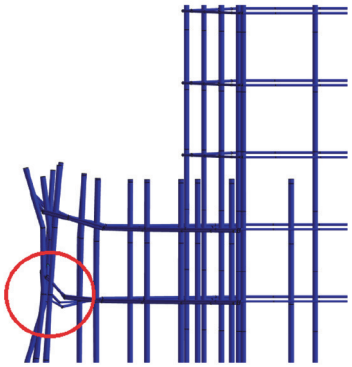 | - | 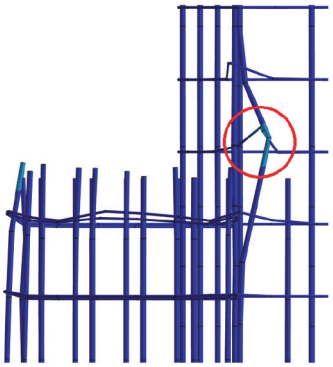 |

the vessel and column. Thus, by using frictionless contact and reducing potential numerical instability, the model completes the calculation within 150 ms for all three considered load case scenarios.

Based on the numerical simulation results presented in Table 5 the most significant volume damage to the column occurs in load case A. In this case, the impact is frontal, concentrating energy on a smaller column area and resulting in progressively more severe damage. The damage propagates in a triangular shape because the load aligns precisely with the plane of the strengthened edge, leaving most of the column undamaged. The concrete exceeds its ultimate strength limit, resulting in significant local material loss and the separation of numerous concrete elements. In contrast, load case B also involves a frontal impact; however, the vessel sails upstream at approximately half the speed of load case A. Consequently, there is no concrete separation during the observed impact duration, and the damage to the column is significantly less extensive. The damage spreads elliptically due to the absence of strengthening on the column's downstream side. Load case C involves an angled impact, distributing the load over a larger surface area. This causes the damage to expand uniformly in all directions, leading to concrete failure. Over time, extensive damage progressively affects a larger area, unlike the more localised but more profound damage observed in frontal impacts.

It has been observed that during a frontal impact, the most significant deformation occurs in the transverse reinforcement. In contrast, the deformation of both transverse and longitudinal reinforcements is roughly equal during an angled impact. This is because the bow contacts the entire strengthened surface of the column, causing both transverse and longitudinal reinforcements to deform inward.

Based on Table 6 it can be concluded that reinforcement yielding occurs first in load case C, which involves an angled impact. Initially, one row of transverse reinforcement yields, followed by one longitudinal reinforcement bar yielding. In load case B, which represents upstream navigation with a frontal impact, there is neither yielding nor significant reinforcement deformation; conversely, in load case A, which involves downstream navigation, the reinforcement experiences maximum deformation precisely at the strengthened region of the column, directly in the impact zone. Yielding of the reinforcement occurs only in the final load cycle and is limited to a single row of transverse reinforcement.

Table 7 shows the change in normal stresses on the bow body. For all load cases, an uneven distribution of stress prevails. The maximum tensile stress is located on the side plate of the bow during a frontal impact downstream (case A) and is equal to 516 MPa. The highest compressive stress also occurs in a frontal downstream impact, reaching 442 MPa. In the upstream navigation direction (case B), normal stress intensity is lower than in downstream navigation (case A) due to the reduced speed and lower kinetic energy dissipation between the column and the barge. In the case of an angled impact (case C), even though the impact velocity is the same as the downstream frontal impact (case A), normal stresses are less intense because the impact force spreads over a larger surface area of the column.

During frontal impact, the highest normal stresses occur directly on the impact surface, specifically at the edge where the column is strengthened. In contrast, the highest stresses are found on the upper bow plate during an angled impact. This is because the side plate of the bow remains rigid at the point of contact due to complete column contact, causing the upper plate to bend instead.

In a direct frontal impact, the barge's collision with the column produces localised high stress at the immediate point of contact caused by the vessel's sudden deceleration. This results in higher normal stresses concentrated within a smaller zone. Conversely, angled impact distributes these stresses over a broader area, leading to comparatively lower stress intensity.

**Table 7. Bow stresses for the considered cases**

| Case | Bow stresses, t = 0.15 s |
|---|---|
| A | 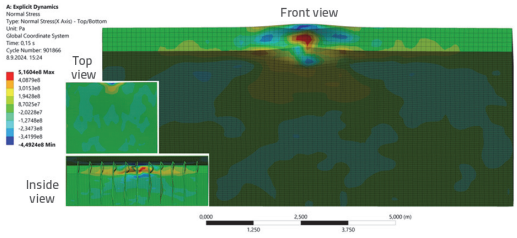 |
| B | 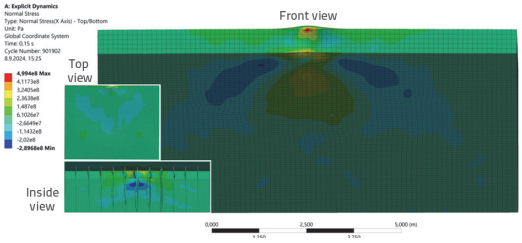 |
| C | 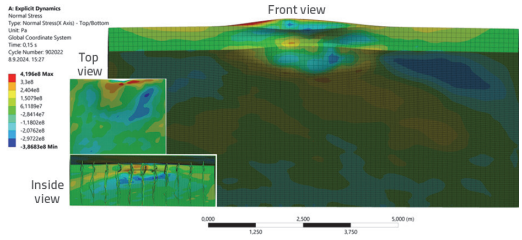 |



## 5. Conclusion

The numerical analysis of a low-energy vessel–bridge collision involving the Ilok–Bačka Palanka Bridge demonstrates the importance of advanced dynamic modelling for assessing structural response under impact. The simulation of the real incident reproduced the main features of the observed column damage, which, based on visual inspection, was classified as superficial: the erosion of the concrete cover exposed reinforcement bars to environmental influence but did not compromise the overall bridge stability.

The adopted model incorporates several simplifications that should be considered when interpreting the results. Soil–structure interaction was omitted, with the pier base idealised as fully fixed and the column top represented through a simplified restraint from the superstructure. The superstructure was represented solely by an equivalent vertical load, without accounting for its full inertia or stiffness. Reinforcement was modelled using beam elements with a perfect bond assumption, neglecting bond–slip effects. Frictional contact modelling suffered from numerical instabilities, requiring both frictionless and frictional simulations, which may affect the accuracy of peak reaction forces. The geometric strain threshold for concrete erosion was adopted from the literature and validated through limited sensitivity checks. Still, its interaction with mesh size suggests that further calibration could lead to a different set of appropriate combinations. Finally, validation was limited by the absence of quantitative field measurements, so comparisons were based on observed damage patterns rather than detailed response histories. The presented results should therefore be interpreted with consideration of the limited availability of measured post-collision data, the use of design-based rather than in-situ material properties, the simplified representation of boundary conditions and superstructure effects, and the need to use a frictionless contact formulation for stable comparative simulations.

Given the low-impact energy, these simplifications were suitable for capturing the essential collision mechanics while maintaining computational efficiency. Despite these limitations, the modelling framework provides meaningful insights into local damage mechanisms and offers a conservative basis for assessing bridge pier performance under vessel collision. The results indicate that, for the investigated bridge, frontal downstream impacts generate the most severe column demands, characterised by concentrated stresses and reinforcement yielding. In contrast, oblique collisions may represent a potentially unfavourable loading scenario due to their ability to redistribute impact forces and engage a broader portion of the structural system. Frictional contact modelling was found to reproduce observed behaviour better, underlining the importance of including realistic contact conditions. Moreover, angled impacts distribute damage over a wider area, reducing local spalling but increasing reinforcement requirements. To enable a more realistic post-impact assessment of bridge stability, especially in high-energy collision scenarios where load-bearing capacity and/or serviceability are threatened, future actions should combine additional field data with an extended numerical model. Recommended actions include:

- As-built geometry and damage survey: perform a detailed geometric survey of the impacted pier (above- and underwater), bearings and the locally thickened concrete region, together with quantitative mapping of damage (height/width/depth), residual cracking and reinforcement exposure.
- In-situ material and durability characterisation: conduct non-destructive testing and/or core extraction where feasible to determine compressive strength, modulus, density and relevant durability indicators (carbonation/chlorides), complemented by a corrosion-condition survey.
- Global structural representation: extend the model to explicitly include the superstructure–bearing–pier system with realistic stiffness, inertia and bearing-level load transfer, so that global response and restraint conditions are represented more faithfully.

- Foundation and riverbed effects: incorporate soil–foundation interaction for the piles, riverbed conditions and potential scour, to capture load redistribution and support compliance under impact.
- Refined vessel–contact modelling: introduce a more detailed vessel/bow representation (structural details, mass distribution, cargo condition) and apply regularised frictional contact formulations to capture tangential effects while avoiding premature numerical instability.
- Residual-performance evaluation and monitoring: include reinforcement–concrete interaction effects (bond–slip/cracking) and assess residual capacity and serviceability indicators (residual stiffness, deflections, crack widths, bearing displacements and vibration characteristics).

Overall, the adopted finite element approach, incorporating advanced material models, is effective at capturing the complex interactions between vessels and structures in low-energy collision scenarios.
These support improved design strategies and risk assessments, particularly for bridges situated along heavily trafficked inland waterways.

## REFERENCES


[1] Wardhana, K., Hadipriono Fabian, C.: Analysis of Recent Bridge Failures in the United States, Journal of Performance of Constructed Facilities, 17 (2003) 3, pp. 144-50.

[2] Knott, M.A., Winters, M.: Ship and barge collisions with bridges over navigable waterways, 2018.

[3] Xu, M.C., Wang, T., Pan, J.: A review on the assessment methods of bridge against ship collision. Thin-Walled Structures, (2024) 205, Paper No. 112347.

[4] EN1991-1-7:2006/A1:2014. Eurocode 1: Actions on structures - Part 1-7: General actions - Accidental actions, European Committee for Standardization (CEN).

[5] Aashto, L.: AASHTO LRFD bridge design specifications. American Association of State Highway and Transportation Officials, Washington, DC, 2012.

[6] Zhang, W.Z., Pan, J., Sanchez, J.C., Li, X.B., Xu, M.C.: Review on the protective technologies of bridge against vessel collision, Thin-Walled Structures, (2024) 201, Paper No. 112013.

[7] Consolazio, G.R., Lehr, G.B., Cook, R.A.: Barge Impact Testing of the St. George Island Causeway Bridge: Phase I: Feasibility Study, 2002.

[8] Consolazio, G.R., Cowan, D.R., Biggs, A., Cook, R.A., Ansley, M., Bollmann, H.T.: Full-Scale Experimental Measurement of Barge Impact Loads on Bridge Piers. Transportation Research Record, 1936 (2005) 1, pp. 80-93.

[9] Chu, L.M., Zhang, L.M.: Centrifuge Modeling of Ship Impact Loads on Bridge Pile Foundations. Journal of Geotechnical and Geoenvironmental Engineering, 137 (2011) 4, pp. 405-420.

[10] Sha, Y., Hao, H.: Laboratory tests and numerical simulations of barge impact on circular reinforced concrete piers. Engineering Structures, 46 (2013), pp. 593-605.

[11] Luperi, F.J., Pinto, F.: Structural Behavior of Barges in High-Energy Collisions against Bridge Piers. Journal of Bridge Engineering, 21 (2016) 2, Paper No. 04015049.

[12] Pu, Q., Liu, J., Gou, H., Bao, Y., Xie, H.: Finite element analysis of long-span rail-cum-road cable-stayed bridge subjected to ship collision. Advances in Structural Engineering, 22 (2019) 11, pp. 2530-4542.

[13] Gholipour, G., Zhang, C., Mousavi, A.A.: Nonlinear numerical analysis and progressive damage assessment of a cable-stayed bridge pier subjected to ship collision. Marine Structures, 69 (2020), Paper No. 102662.

[14] Kantrales, G.C., Consolazio, G.R., Wagner, D., Fallaha, S.: Experimental and Analytical Study of High-Level Barge Deformation for Barge–Bridge Collision Design, Journal of Bridge Engineering, 21 (2016) 2, Paper No. 04015039.

[15] Gholipour, G., Zhang, C., Li, M.: Effects of soil–pile interaction on the response of bridge pier to barge collision using energy distribution method, Structure and Infrastructure Engineering, 14 (2018) 11, pp. 1520-1534.

[16] McVay, M.C., Wasman, S.J., Consolazio, G.R., Bullock, P.J., Cowan, D.G., Bollmann, H.T.: Dynamic Soil–Structure Interaction of Bridge Substructure Subject to Vessel Impact, Journal of Bridge Engineering, 14 (2009) 1, pp. 7-16.

[17] Sha, Y., Hao, H.: Nonlinear finite element analysis of barge collision with a single bridge pier, Engineering Structures, 41 (2012), pp. 63-76.

[18] Fan, W., Shen, D., Huang, X., Sun, Y.: Reinforced concrete bridge structures under barge impacts: FE modeling, dynamic behaviors, and UHPFRC-based strengthening, Ocean Engineering, 216 (2020), Paper No. 108116.

[19] Gholipour, G., Zhang, C., Mousavi, A.A.: Effects of axial load on nonlinear response of RC columns subjected to lateral impact load: Ship-pier collision, Engineering Failure Analysis, 91 (2018), pp. 397-418.

[20] Cowan, D.R., Consolazio, G.R., Davidson, M.T.: Response-Spectrum Analysis for Barge Impacts on Bridge Structures, Journal of Bridge Engineering, 20 (2015) 12, Paper No. 04015017.

[21] Fan, W., Yuan, W.C.: Shock spectrum analysis method for dynamic demand of bridge structures subjected to barge collisions, Computers & Structures, 90-91 (2012), pp. 1-12.

[22] Guo, X., Zhang, C., Chen, Z.: Experimental and numerical assessment of scoured bridges with protective bonded steel plates against vessel impact, Engineering Structures, 252 (2022), Paper No. 113628.

[23] Zhu, L., Liu, W., Fang, H., Chen, J., Zhuang, Y., Han, J.: Design and simulation of innovative foam-filled Lattice Composite Bumper System for bridge protection in ship collisions, Composites Part B: Engineering, 157 (2019), pp. 24-35.

[24] Consolazio, G.R., Davidson, M.T.: Simplified Dynamic Analysis of Barge Collision for Bridge Design, Transportation Research Record, 2050 (2008) 1, pp. 13-25.

[25] Davidson, M.T., Consolazio, G.R., Getter, D.J.: Dynamic Amplification of Pier Column Internal Forces Due to Barge–Bridge Collision,Transportation Research Record, 2172 (2010) 1, pp. 11-22.

[26] Davidson, M.T., Consolazio, G.R., Getter, D.J., Shah, F.D.: Probability of Collapse Expression for Bridges Subject to Barge Collision, Journal of Bridge Engineering, 18 (2013) 4, pp. 287-296.

[27] ANSYS: Ansys engineering analysis system user's manual, 2024.

[28] Arhiv: Glavni projekt drumskog mosta preko rijeke Dunava kod Bačke Palanke, Fond 2065, Državni arhiv u Zagrebu, 1971.

[29] MMPI - Ministry of the sea, transport and infrastructure: https://mmpi.gov.hr/more-86/unutarnja-plovidba-rijecni-promet/priopcenja-za-brodarce/lucka-kapetanija-vukovar/14964, 2024.

[30] Rinker, M.W., Pilli, S.P., Karri, N.K., Deibler, J.E., Johnson, K.I., Holbery, J.D., et al.: Structural integrity of single shell tanks at Hanford-9491, WM2009 Conference, 2009.

[31] Zhao, W., Zhu, B.: Theoretical model for the bond–slip relationship between ribbed steel bars and confined concrete, Structural Concrete, 19 (2018) 2, pp. 548-58.

[32] Mohammed, H.D., Jabbar, M.A., Hasan, A.Q.: Experimental and Numerical Behavior of Basalt Fiber Reinforced Short Concrete Columns Under Axial Loading. Periodica Polytechnica Civil Engineering, 68 (2024) 1, pp. 23-36.

[33] Guo, Q., Chen, Q.-w., Xing, Y., Xu Y.N., Zhu, Y.: Experimental Study of Friction Resistance between Steel and Concrete in Prefabricated Composite Beam with High-Strength Frictional Bolt. Advances in Materials Science and Engineering, 1 (2020), Paper No. 1292513.

[34] Riedel, W., Thoma, K., Hiermaier, S.: Penetration of reinforced concrete by BETA-B-500 numerical analysis using a new macroscopic concrete model for hydrocodes. In: Proceedings of 9th, ISIEMS; 1999. Berlin.

[35] EN 206-1:2026. Concrete - Specification, performance, production and conformity - Part 1: Performance, requirements, factory production control and assessment criteria for individual values (EN 206-1:2026), European Committee for Standardisation (CEN).

[36] Luccioni B.M., Aráoz G.F., Labanda N.A.: Defining Erosion Limit for Concrete, International Journal of Protective Structures, 4 (2013) 3, pp. 315-340.

[37] Draganić, H., Jeleč, M., Gazić, G., Lukić, S.: Numerical Investigations of Reinforced Concrete Slabs Subjected to Contact Explosions. Buildings, 15 (2025) 7, Paper No. 1063.

[38] Johnson, G., Cook, W.: Selected hugoniots: EOS, 7th International Symposium on Ballistics, 1969, LA-4167-MS.